NEURODEGENERATION

Pin1 mediates $A\beta_{42}$-induced dendritic spine loss

Nancy R. Stallings,[1]* Melissa A. O'Neal,[1]* Jie Hu,[1] Ege T. Kavalali,[2] Ilya Bezprozvanny,[3] James S. Malter[1]†

Early-stage Alzheimer's disease is characterized by the loss of dendritic spines in the neocortex of the brain. This phenomenon precedes tau pathology, plaque formation, and neurodegeneration and likely contributes to synaptic loss, memory impairment, and behavioral changes in patients. Studies suggest that dendritic spine loss is induced by soluble, multimeric amyloid-β ($A\beta_{42}$), which, through postsynaptic signaling, activates the protein phosphatase calcineurin. We investigated how calcineurin caused spine pathology and found that the cis-trans prolyl isomerase Pin1 was a critical downstream target of $A\beta_{42}$-calcineurin signaling. In dendritic spines, Pin1 interacted with and was dephosphorylated by calcineurin, which rapidly suppressed its isomerase activity. Knockout of Pin1 or exposure to $A\beta_{42}$ induced the loss of mature dendritic spines, which was prevented by exogenous Pin1. The calcineurin inhibitor FK506 blocked dendritic spine loss in $A\beta_{42}$-treated wild-type cells but had no effect on *Pin1*-null neurons. These data implicate Pin1 in dendritic spine maintenance and synaptic loss in early Alzheimer's disease.

INTRODUCTION

Early stages of Alzheimer's disease (AD) or mild cognitive impairment are characterized by memory loss and behavioral changes. These symptoms likely reflect loss of dendritic spines and their synaptic connections induced by soluble, multimeric amyloid-β ($A\beta_{42}$) (*1*, *2*). Spine and synaptic loss occurs before neurodegeneration or tau pathology, suggesting that spine preservation strategies could attenuate or prevent AD progression (*1*). It is not clear how regulators of spine maintenance are negatively affected during the development of AD by increased, soluble $A\beta_{42}$.

One protein whose dysfunction is implicated in both spine physiology and AD pathogenesis is the peptidyl-prolyl isomerase Pin1 (*3*). Pin1 binds to and catalyzes the cis-to-trans conversion of amyloid precursor protein (APP), phosphorylated tau (p-tau), and other postsynaptic proteins at phosphoserine (pSer)/pThr-Pro bonds, altering their function and/or catabolism (*4*). Target binding is mediated through an N-terminal, WW domain, whereas isomerization occurs through a C-terminal enzymatic domain. Ser or Thr phosphorylation, typically by proline-directed kinases, such as mitogen-activated protein kinase (MAPK), protein kinase C (PKC), and cyclin-dependent kinase (CDK) families, accelerates Pin1-mediated isomerization of peptide bond by approximately 1000-fold (*5*). Under basal conditions, Pin1 is highly active in neuronal cell bodies, nuclei, axonal growth cones, and dendritic spines but can be inhibited by glutamatergic, outside-in signaling that induces phosphorylation of Ser^{16} within the WW binding domain, preventing target recognition (*6*). Most relevant to AD, Pin1-mediated isomerization drives APP cleavage toward the α and away from the β/γ secretase pathway, reducing $A\beta_{42}$ production (*7*, *8*). By binding to and isomerizing p-tau, Pin1 also prevents neurofibrillary tangle formation (*4*), again suggesting a possible role for its dysfunction in AD pathogenesis.

Consistent with this hypothesis, cortical Pin1 protein content (*7*) and activity (*9*) are often reduced or lost in end-stage AD, whereas germline *Pin1* knockout (KO) accelerates AD pathology in Tg2576 mice, which overproduce $A\beta_{42}$ (*8*). The isomerase activity of Pin1 is lost due to oxidation of Cys^{113}, a critical amino acid within its active site (*9*). Whether alterations in inside-out signaling, especially at synaptic sites, can affect Pin1 activity or steady-state protein amounts during AD evolution is unknown.

Somewhat paradoxically, hippocampal slices from pure-background, germline *Pin1* KO mice display increased, rather than reduced, long-term potentiation (LTP) (*10*) and show increased, rather than decreased, hippocampal dendritic spine density (*6*), phenotypes that are opposite than is predicted from the pathology seen in AD or murine AD models. Pure-background *Pin1* KO mice are very difficult to breed, with only ~2 to 5% of the expected viable births. These discrepancies suggested that viable KO mice somehow complemented for the loss of Pin1, masking the true effects of gene ablation. This encouraged us to develop $Pin1^{fl/fl}$ mice so that Pin1 loss could be assessed after development in vivo and in vitro. Using floxed mice and neuronal cultures derived from them, we found that Pin1 is required to maintain mature dendritic spines, and that postsynaptic Pin1 is inhibited by soluble, multimeric $A\beta_{42}$-mediated signaling through calcineurin, and that this event causes spine loss. These results suggest that Pin1 can be inactivated early in the evolution of AD by $A\beta_{42}$ signaling that directly contributes to spine pathology. The results also suggest that previous data from germline *Pin1* KO mice should be carefully reassessed.

RESULTS

Neocortices from AD patients show progressive losses of Pin1 along with synapses and dendritic spines (*11*) that can be mimicked in cultured neurons (*12*) or slice preparations (*13*) treated with multimeric $A\beta_{42}$. Unexpectedly, germline *Pin1* KO cortex tissues exhibit increased dendritic spine density and increased LTP in hippocampal slices (*6*, *10*). To clarify these seemingly contradictory results, we measured total dendritic spine density of primary DIV21 (21 days in vitro) $Pin1^{fl/fl}$ neurons after transfection on DIV7 with Td-Tomato and either nuclear localization signal (NLS)–green fluorescent protein (GFP) (WT) or NLS-GFP-Cre (KO) (fig. S1A). Spine counts were reproducibly 35% lower in Pin1 KO versus WT cultures (3.04 ± 0.39 per 10 μm compared to 4.77 ± 0.25 per 10 μm) (Fig. 1A and fig. S1, B and C), with significant reductions in mature mushroom and stubby spines

[1]Department of Pathology, University of Texas Southwestern Medical Center, 5323 Harry Hines Boulevard, Dallas, TX 75390, USA. [2]Department of Neuroscience, University of Texas Southwestern Medical Center, Dallas, TX 75390, USA. [3]Department of Physiology, University of Texas Southwestern Medical Center, Dallas, TX 75390, USA.
*These authors contributed equally to this work.
†Corresponding author. Email: james.malter@utsouthwestern.edu

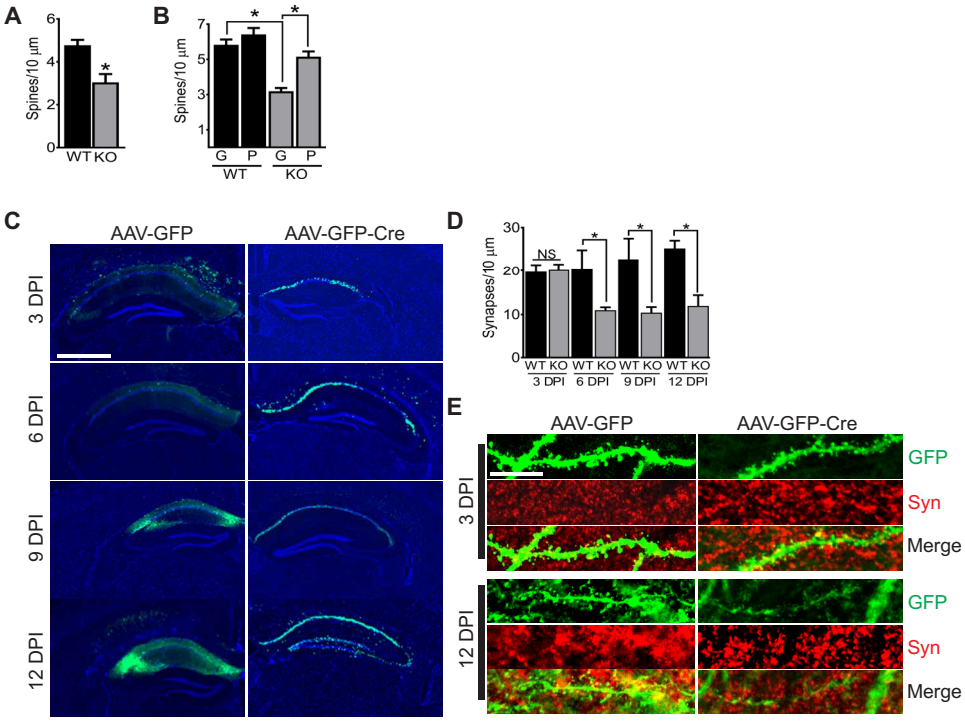

Fig. 1. Pin1 KO causes dendritic spine loss in vitro and vivo. (**A**) Total spine counts in Pin1$^{fl/fl}$ neurons after transfection with Td-Tomato and either NLS-GFP [wild-type (WT), black] or NLS-GFP-Cre (KO, gray). Neurons were fixed at DIV21. (**B**) As described in (A), in DIV21 neurons transduced with TAT-GFP ("G") or TAT-Pin1 ("P"). (**C**) Representative images of GFP immunofluorescence in hippocampi of AAV-GFP– or AAV-GFP-Cre–injected 3-month-old Pin1$^{fl/fl}$ mice at 3, 6, 9 and 12 DPI. Sections were counterstained with DAPI. Scale bar, 1000 μm. (**D**) Total synapse counts at 3, 6, 9, and 12 DPI from 24 mouse hippocampi injected at 3 months old with either AAV-GFP (WT, black) or AAV-GFP-Cre (KO, gray). (**E**) Imaging of GFP (green) and antibody to synaptophysin (Syn; red) in dendritic spines from hippocampal neurons described in (C). A representative composite *Z*-stack image of three 0.33-μm-thick step sizes is shown. Scale bar, 10 μm. Data are means ± SEM; $n > 100$ spines from ≥15 images and ≥3 coverslips per condition were counted. $^*P < 0.05$ by an unpaired *t* test (A) or Fisher's least significant difference (LSD) test following two-way analysis of variance (ANOVA) (B and C). NS, not significant.

(fig. S1C). To verify the results seen in genetically modified cells, we exposed cultured neurons to recombinant WW domain fused to the transactivator of transcription (TAT) tag (TAT-WW), which we and others have previously established would enter spines directly, very rapidly, and with minimal toxicity (*10*, *14*, *15*). TAT-WW functions as a dominant-negative, preventing endogenous Pin1 from binding to target proteins (*16*). Spine counts were similarly reduced in WT cells transduced with TAT-WW (fig. S1, D to F) but were restored to normal in KO cells after transduction with recombinant TAT-Pin1 (Fig. 1B and fig. S1, G and H). To control for nonspecific effects of TAT, neurons were also transduced with TAT-GFP. These cells showed no changes in spine counts or spine types from untreated, control neurons (fig. S1, D to F). Therefore, postdevelopmental Pin1 loss or inhibition caused loss of mature dendritic spines that could be rescued by exogenous TAT-Pin1 but not TAT-GFP.

To determine whether Pin1 was required for spine stability in vivo, we injected adeno-associated virus (AAV)–GFP–Cre or AAV-GFP into the hippocampus of adult Pin1$^{fl/fl}$ mice (Fig. 1C). Synapse numbers in projections from GFP and synaptophysin co-positive CA1 hippocampal neurons were unchanged between the controls and KO mice at 3 days post-injection (DPI) but were significantly decreased (~40%) by 6 DPI in Pin1 KO neurons (Fig. 1, D and E). Laser-captured, microdissected GFP-positive hippocampal cells were analyzed by polymerase chain reaction for recombination. Hippocampi injected with AAV-GFP-Cre showed substantial recombination that was not seen in the thalamus of these animals or in mice injected with AAV-GFP (fig. S2A). Thus, Pin1 loss both in vitro and in vivo caused spine loss.

We next assessed Pin1 abundance and isomerase activity in soluble fractions from fresh-frozen, frontal cortex tissue from AD patients and from age-matched individuals who were not diagnosed with cognitive deficit (fig. S2B). The abundance of Pin1 and βIII-tubulin protein was consistently reduced in AD samples, whereas the abundance of synaptosomal-associated protein 25 (SNAP25), a commonly used measure of synaptic number (*17*), was more variable compared to normal, age-matched controls (Fig. 2A) (*7*). Protease-coupled isomerase assay (*18*) specific for Pin1 revealed significantly reduced isomerase activity in AD brain lysates compared to controls (Fig. 2B). However, given the amount of immunoreactive protein, Pin1 activity was less than expected in AD samples. These data suggested that Pin1 was somehow inactivated in AD lysates. Pin1 can be oxidized at Cys^{113}, blocking activity (*9*) or inhibited by outside-in glutamatergic signaling (*10*). To identify the mechanism, we used mouse synaptoneurosomes (SNs), a highly enriched preparation of pre- and postsynaptic neuronal connections from brain. Isomerase activity was measured in control SNs or after incubation with soluble AD brain lysates or age-matched control lysates. Control brain lysates had no effect on Pin1 activity, but AD lysates significantly suppressed activity (Fig. 2C). We were able to entirely replicate these findings with 100 nM multimerized, soluble Aβ_{42} (fig. S2C) or with PiB, TAT-WW, or juglone, all established Pin1 inhibitors (Fig. 2D) (*12*). TAT-W34A, which contains an inactivating mutation of the terminal tryptophan in the WW domain, had no effect (Fig. 2D), demonstrating that Pin1 activity in SNs was not affected by TAT-mediated transduction. These data demonstrate that synaptic Pin1 can be inhibited by soluble, multimeric Aβ_{42} signaling.

On the basis of the results, we determined the effects of Aβ_{42} on dendritic spines in Pin1 KO and WT neurons. As expected, Aβ_{42} significantly reduced total and stubby spine density of WT neurons to the numbers seen in untreated KO cells (Fig. 3A and fig. S3, A and B). Neither Aβ_{42} nor TAT-GFP had a significant effect on the total spine density of KO neurons (Fig. 3B and fig. S3, C and D). The spines of WT neurons transduced with excess TAT-Pin1 were fully resistant to Aβ_{42} (Fig. 3A and fig. S3, A and B), whereas KO cultures treated with TAT-Pin1 were partially sensitive to Aβ_{42} (Fig. 3B and fig. S3, C and D). Therefore, Pin1 plays a previously unappreciated role in dendritic spine maintenance and its loss phenocopied spine alterations

seen in neurons exposed to multimeric $A\beta_{42}$. These results strongly suggest that $A\beta_{42}$ signaling causes spine loss by inhibiting Pin1.

Phosphorylation of Pin1 at Ser^{16}, Ser^{71}, or Ser^{138} alters activity (*16*, *19*, *20*). We immunoprecipitated (IP) Pin1 from SNs after brief treatment (10 min) with $A\beta_{42}$ and analyzed for interactions and post-translational modifications (PTMs) by mass spectrometry (MS). Calcineurin subunits were reproducibly associated with Pin1 by MS (fig. S3E) that was confirmed by IP/immunoblotting (Fig. 3C). $A\beta_{42}$ induced Pin1 dephosphorylation at Ser^{111}, Ser^{147}, and Ser^{154}, sites not previously reported as modified. As seen in primary cortical neurons, dendritic spines, and N2A cells (*21*, *22*), we confirmed that $A\beta_{42}$ quickly increased calcineurin activity in SNs (Fig. 3D). We therefore asked whether the calcineurin inhibitor FK506 or cyclosporin A (CsA) could attenuate $A\beta_{42}$-mediated suppression of Pin1 activity in SNs. FK506 at 3 nM [median inhibitory concentration (~IC_{50})] or CsA at 5 nM (~IC_{50}) completely prevented the suppression of Pin1 isomerase activity by $A\beta_{42}$ (Fig. 3E). Therefore, calcineurin binds to and likely dephosphorylates Pin1 at Ser^{111}, Ser^{147}, and/or Ser^{154} in response to $A\beta_{42}$ signaling, possibly altering Pin1 activity.

Application of FK506 restored spine numbers and complexity in neurons exposed to $A\beta_{42}$ in vivo (*23*) and in vitro (*24*). The dendritic targets of calcineurin that are required for spine maintenance are largely unknown. As expected, FK506 completely rescued spine numbers and maturity in WT cells treated with $A\beta_{42}$ (Fig. 4A and fig. S4, A and B) but had no effect on spine numbers in Pin1 KO cells irrespective of $A\beta_{42}$ treatment (Fig. 4A and fig. S4, A and C). Therefore, $A\beta_{42}$ and calcineurin signaling inhibit Pin1 whose activity is required for spine maintenance. Therapeutics such as FK506 that block calcineurin and preserve Pin1 activity could potentially be effective in attenuating spine losses in early AD.

Ser^{111} is in very close proximity to the active-site Cys^{113} (*25*, *26*). Thus, TAT-GFP (TAT control), TAT-Pin1, TAT-Pin1-S111A (phospho-null), or TAT-Pin1-S111D (phospho-mimetic) recombinant proteins were produced and added to SNs or to Pin1 WT and KO neurons, and isomerase activity or spine numbers were determined. TAT-Pin1-S111D–transduced SNs were completely resistant to $A\beta_{42}$, whereas TAT-Pin1-S111A functioned as a dominant-negative similar to C113A (Fig. 4B and fig. S5A). TAT-GFP had no effect on Pin1 activity or responsiveness to $A\beta_{42}$ (Fig. 4B and fig. S5A). TAT-Pin1-S111A significantly reduced spine numbers in WT cultures to the same degree as $A\beta_{42}$ or as seen in untreated KO neurons (Fig. 4, C and D, and fig. S5, B to K). Conversely, TAT-Pin1 or TAT-Pin1-S111D had no effect on control WT cells but significantly increased spine counts in WT neurons treated with $A\beta_{42}$ or untreated KO neurons (Fig. 4, C and D, and fig. S5, B to K). However, only TAT-Pin1-S111D was reproducibly able to rescue spine counts in KO cells treated with $A\beta_{42}$ (Fig. 4D and figs. S4C and S5, H to K). In aggregate, these results suggest that $A\beta_{42}$ induces calcineurin to dephosphorylate Pin1 at Ser^{111}, rendering it inactive. Pin1-S111D is constitutively active, is resistant to $A\beta_{42}$ signaling and calcineurin-mediated dephosphorylation, and supports spine numbers and complexity in both WT and KO neurons.

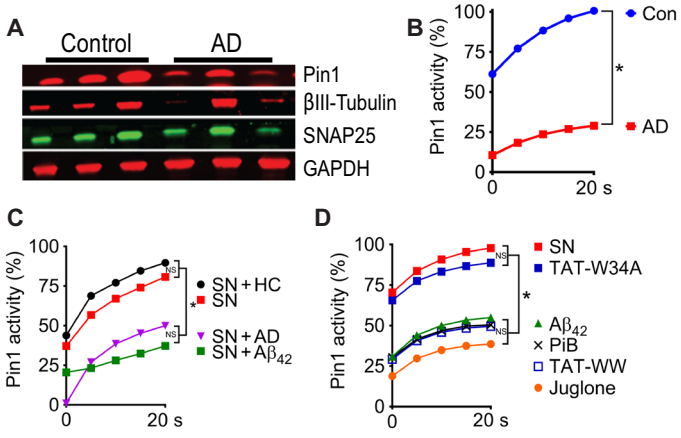

Fig. 2. $A\beta_{42}$ inhibits Pin1 isomerase activity. (**A**) Western blotting for Pin1, SNAP25, βIII-tubulin, and GAPDH (glyceraldehyde-3-phosphate dehydrogenase) in soluble fractions of temporal cortex lysates from three Alzheimer's disease (AD) patients and three age-matched control individuals (not diagnosed with dementia; Con). (**B**) Pin1 activity assay in equal amounts of soluble protein extract from control and AD patient brain tissues described in (A). (**C**) Pin1 activity assay with murine SNs that were untreated (red) or treated for 10 min with control brain extract (+HC; black), AD brain extract (+AD; purple), or $A\beta_{42}$ (green). (**D**) Pin1 activity assay in SNs that were either untreated (red) or treated with juglone, PiB, TAT-WW, TAT-W34A, or $A\beta_{42}$. Data are means of $n \geq 8$ replicates per treatment. *$P < 0.05$ by Fisher's LSD test following two-way ANOVA (B to D).

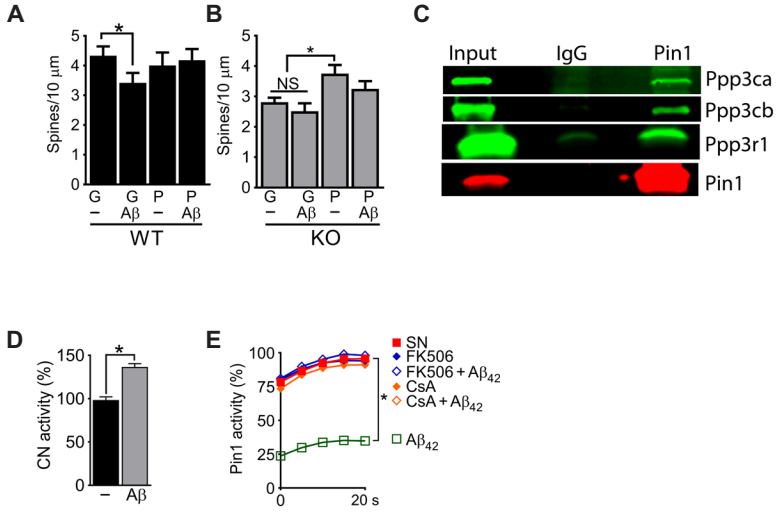

Fig. 3. Calcineurin interacts with Pin1 and mediates $A\beta_{42}$ signaling. (**A** and **B**) Total spine counts for DIV21 WT (A) or DIV21 KO (B) neurons transduced with TAT-GFP ("G") or TAT-Pin1 ("P") ± $A\beta_{42}$ (Aβ). Data are means ± SEM; $n > 100$ spines from ≥15 images and ≥3 coverslips per condition were counted. *$P < 0.05$ by Fisher's LSD test following two-way ANOVA. (**C**) Western blot of catalytic and regulatory subunits of calcineurin in Pin1 immunoprecipitations from SNs prepared from P28 mice. (**D**) Calcineurin (CN) activity in SNs that were either untreated (–) or treated with $A\beta_{42}$ (Aβ) for 10 min before lysis. Data are means ± SEM; n = 3 biological replicates. *$P < 0.05$ by an unpaired t test. (**E**) Pin1 activity assay in SNs that were either untreated (SN) or treated with $A\beta_{42}$, FK506, FK506 + $A\beta_{42}$, CsA, or CsA + $A\beta_{42}$ before lysis. Data are means from $n \geq 8$ replicates per treatment. *$P < 0.05$ by Fisher's LSD test following two-way ANOVA.

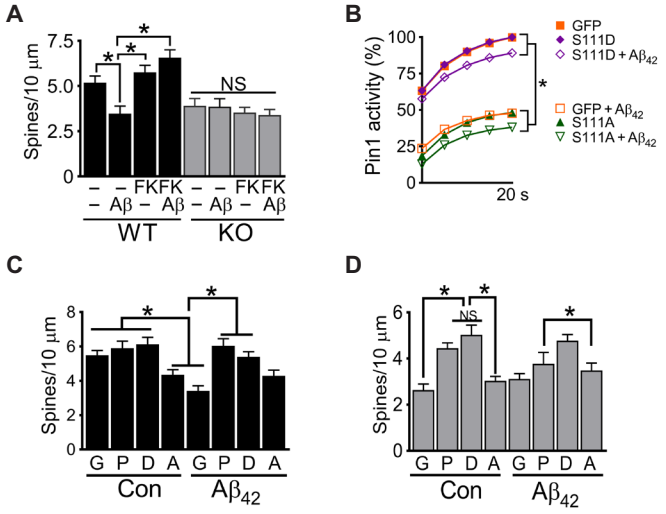

Fig. 4. Dephosphorylation of Pin1 at Ser^{111} inhibits Pin1 activity. (**A**) Total spine counts for DIV21 WT (black) or KO (gray) neurons ± FK506 (FK) ± $A\beta_{42}$ (Aβ). (**B**) Pin1 activity assay in SNs treated with TAT-GFP (GFP), TAT-Pin1-S111D (S111D), or TAT-Pin1-S111A (S111A) ± $A\beta_{42}$ before lysis. Data are means from $n \geq 8$ replicates per treatment. *$P < 0.05$ by Fisher's LSD test following two-way ANOVA. (**C** and **D**) Total spine counts in DIV21 WT (C) and KO (D) neurons transduced with TAT-GFP ("G"), TAT-Pin1 ("P"), TAT-Pin1-S111A ("A"), or TAT-Pin1-S111D ("D") ± $A\beta_{42}$. Data are means ± SEM; $n > 100$ spines from ≥15 images and ≥3 coverslips per condition were counted. *$P < 0.05$ by Fisher's LSD test following two-way ANOVA (A, C, and D).

DISCUSSION

One of the earliest pathologic events in evolving AD is the loss of synapses and dendritic spines (*27*). These changes presumably underlie initial memory and behavioral deficits and occur before neuronal losses or neurofibrillary tangle formation (*27*). The work presented here demonstrates that a signaling cascade initiated by soluble $A\beta_{42}$ leads to calcineurin activation and Pin1 inhibition, negatively affecting dendritic spine health. Furthermore, the data suggest that calcineurin inhibitors such as FK506 could attenuate spine loss due to $A\beta_{42}$ signaling, potentially reducing early AD symptoms. Because spine loss can accelerate neuronal death (*25*), spine sparing strategies could also slow AD development.

Pin1 can regulate $A\beta_{42}$ production and p-tau accumulation (*3*, *7*, *8*, *28*). Discrepancies between spine counts and LTP in germline Pin1 KO and AD model mice that lose Pin1 over time led us to create and study Pin1$^{fl/fl}$ mice. Postnatal Pin1 loss caused a significant decrease in spine density that could be rapidly rescued by the transduction of exogenous Pin1. Corroborating data were seen in Pin$^{fl/fl}$ adult mice after intrahippocampal delivery of AAV-GFP-Cre, confirming that Pin1 is required for dendritic spine maintenance in mature neurons. The differences in spine density phenotype in germline and conditional KO cells suggest that Pin1 has distinct functions in dendritic spine development and spine maintenance. At this point, we do not know whether other observed phenotypes in germline KO mice including impaired numbers and differentiation of neural progenitor cells, growth cone abnormalities, and misorganization of global brain architecture (*6*, *29*–*31*) accurately reflect Pin1's role in neurodevelopment.

Pin1 activity is sensitive to outside-in glutamatergic signaling (*10*), but the regulation by $A\beta_{42}$ signaling has not been previously shown. These effects were observed with multimeric $A\beta_{42}$, a phenotype similar to the suppressive effects on LTP in slices, dendritic spine density, and neurotoxicity in culture (*1*, *2*, *30*). Multimeric, soluble $A\beta_{42}$ causes a variety of postsynaptic signaling abnormalities including alteration of Ca^{2+} homeostasis involving both intracellular and extracellular stores (*32*). Calcineurin is a calcium/calmodulin-dependent protein phosphatase highly expressed in normal brain and aberrantly activated in AD patients (*33*–*35*), mouse models, and cultured neurons (*21*, *35*, *36*). Increased calcineurin activity disrupts synaptic networks, reduces LTP (*37*), increases long-term depression (*38*), and decreases memory (*34*, *39*–*41*). On the basis of our data, $A\beta_{42}$-mediated effects on calcineurin can be modeled and studied in SNs, permitting detailed biochemical analysis.

One of the downstream effects of $A\beta_{42}$-mediated calcineurin activation is Pin1 inactivation. These effects are likely direct because Pin1 interacts with multiple calcineurin subunits, and the loss of Pin1 activity can be prevented by mechanistically distinct calcineurin inhibitors FK506 and cyclosporine. FK506 binds FKBP12 to form a complex that inhibits calcineurin activity, whereas CsA forms a complex with cyclophilin A to block calcineurin activity (*42*–*44*). FK506 has been shown to rescue $A\beta_{42}$-induced dendritic spines loss, calcium dysregulation, hippocampal LTP, and behavioral deficiencies in mice (*23*, *32*, *36*, *45*). A retrospective study showed that transplant patients receiving FK506 developed markedly less AD than expected (*36*). Patients immunosuppressed with the mammalian target of rapamycin (mTOR) inhibitor showed the expected incidence of AD, suggesting that calcineurin inhibition, rather than peripheral immunosuppression, was required to reduce AD incidence in transplant patients. Here, FK506 was able to rescue $A\beta_{42}$-mediated dendritic spine loss only in Pin1-replete cultures. Whether Pin1 is also involved in upstream $A\beta_{42}$ signaling that activates calcineurin remains to be determined. If so, our data would predict that Ser^{111}-phosphorylated Pin1 would oppose calcineurin activation by $A\beta_{42}$. Together, these data demonstrate that FK506 rescued $A\beta_{42}$-mediated dendritic spine loss in a Pin1-dependent manner.

The rapid kinetics of $A\beta_{42}$-mediated effects are most consistent with changes in PTMs of Pin1. Phosphorylation at Ser^{16} by PKMζ or PKA (*10*, *16*) or Ser^{71} by DAPK1 (*19*) inhibited Pin1 activity, whereas MLK3-mediated Ser^{138} phosphorylation had the opposite effect (*20*). Polo-like kinase 1 (PLK1) phosphorylation at Ser^{65} stabilized Pin1 protein without alteration of isomerization activity (*46*). The identification of Ser^{111} phosphorylation as required for activity has not been described. This amino acid is within the catalytic pocket of Pin1 and very close to the active-site Cys^{113} (*26*). Phospho-null Pin1-S111A mutants showed dominant-negative activity as previously shown for C113A mutants, whereas phospho-mimetic Pin1-S111D was constitutively active, was fully resistant to $A\beta_{42}$-mediated inhibition, and supported spine counts irrespective of $A\beta_{42}$ treatment. On the basis of the work here and the data of others, we propose that the gradual accumulation of multimeric $A\beta_{42}$ in evolving AD increases calcineurin activity, causing a progressive reduction of Pin1 activity in postsynaptic dendritic spines. Presumably, Pin1 interacts with and is required for the function of protein(s) essential for spine maintenance and complexity. As Pin1 also regulates $A\beta_{42}$ production (*8*), we also propose that Pin1 inhibition accelerates $A\beta_{42}$ production, further suppressing Pin1. The potential for calcineurin inhibition to actively interfere with this feed-forward loop makes it an intriguing therapeutic concept.

MATERIALS AND METHODS

Animals

Pin1$^{fl/fl}$ mice were created using traditional methods (fig. S2A). Pin1$^{fl/fl}$ mice were maintained on a C57/Bl6 background and were bred by

crossing homozygous Pin1$^{fl/fl}$ mice with homozygous Pin1$^{fl/fl}$ mice. Mice were fed a standard chow (Teklad Global 16% Rodent Diet, #2016) ad libitum and were housed in a standard 12-hour light/dark cycle. All animal use was done in accordance with protocols approved by the University of Texas Southwestern (UTSW) Medical Center Institutional Use and Animal Care Committee.

SN preparation

Pin1$^{fl/fl}$ mice in a C57/Bl6 background were used for all SN preparations per the method described in (*12*). Briefly, mouse cortices were harvested from mice that were heavily sedated with 2,2,2-tribromoethanol (Avertin). Using a 5-ml homogenizer, two brains were processed at a time with 10 strokes of pestle A and then pestle B. Combined homogenate was then prepared per the method described in (*10*). SN preps were aliquoted and treated with juglone, PiB, CsA, concatamerized Aβ_{42}, FK506, or TAT proteins purified per (*10*). The reactions were stopped with a final concentration of 1% Triton X-100. Samples were snap-frozen and briefly stored at −80°C until assayed.

Neuronal culture

Cortices from Pin1$^{fl/fl}$ P1 pups were dissected, roughly chopped with a razor blade, and then placed in a 1:1 solution of 0.25% trypsin–Dulbecco's phosphate-buffered saline (DPBS) with 10 U of deoxyribonuclease per milliliter of dissection solution. After 30 min, the digestion was stopped by the addition of minimum essential medium with 20% fetal calf serum. Cells were centrifuged for 5 min at 1000 rpm, supernatant was aspirated, and the cells were washed again with the stop solution. The medium was aspirated, and the cell pellet was resuspended in 2 ml of Neurobasal-A supplemented with B27, L-glutamine, penicillin, streptomycin, and 5% fetal calf serum. Cells were then filtered through 70- and 40-μm filters and then plated on coverslips coated with poly-D-lysine. At DIV7, cultures were transfected with Td-Tomato and NLS-GFP (wild-type) plasmids or Td-Tomato and NLS-GFP-Cre (KO) plasmids using a calcium phosphate method (*47*). The Td-Tomato and NLS-GFP-Cre plasmids were used as previously published (*48*).

DIV21 cultures were treated with 100 nM TAT-Pin1 (WT), TAT-Pin1-S111A, TAT-Pin1-S111D, TAT-WW, TAT-W34A, or TAT-GFP for 3 hours. Aβ_{42} (100 nM) or vehicle was added to the culture for an additional hour. FK506 (5 nM) was added 15 min before Aβ_{42}. Cells were fixed in 4% paraformaldehyde (PFA) and 4% sucrose and analyzed for spine morphology. A *Z* stack was captured using a 100× objective on a Zeiss Axiovert LSM510 confocal microscope or a 63× objective with 2.73 zoom on a Leica DM6000B confocal microscope. An entire experimental data set was analyzed on one microscope. At least 15 *Z* stacks per group were analyzed using NeuronStudio (*49*), with the modifications described (*48*). Briefly, dendrites were traced, and the build spine function was used to identify spines. Computer-generated spine classifications were then manually reviewed by the user, and data were exported to Excel and GraphPad Prism, where statistical analysis was performed. Graphing of data was performed in GraphPad Prism v7.01. For image presentation, representative confocal *Z* stacks were opened in ImageJ, converted to a *Z* project with max intensity, and saved as a .tif file. Images were then rotated and cropped in Photoshop for insertion in the figure.

Pin1 isomerase activity assays

Pin1 substrate (1 mg) (Suc-Ala-Glu-Pro-Phe-pNA, Peptides International) was suspended in 15 μl of DMSO, then diluted 1:100 in 1 M lithium chloride in trifluoroethanol, and allowed to incubate a minimum of 30 min at room temperature (RT). Chymotrypsin was suspended at 100 mg per 1.67 ml of 0.001 N HCl. Final concentration of assay buffer was 50 mM Hepes (pH 7), 100 mM NaCl (pH 7), 2 mM dithiothreitol (DTT), bovine serum albumin (BSA; 0.04 mg/ml), and chymotrypsin (0.03 mg/ml). Frozen SN lysates were thawed on ice. Analysis was performed on a Jasco V630 spectrophotometer with a multiwell accessory at 390 nm. To perform the peptidyl-prolyl cis-trans isomerase (PPIase) assay on SN preps, 100 μl of SN lysate was premixed with 1 ml of assay buffer and incubated at least 30 min in a 25°C heat block. SN lysate (110 μl) was pipetted into the eight wells in the multiwell accessory unit and individually assessed. Each well was blanked while containing the original sample, and then 5 μl of Pin1 substrate was added and the sample was immediately analyzed every 0.1 s for 60 s. The human brain samples were run with 2 μg per assay. Data were exported to GraphPad Prism v7.01 for graphing and analysis. All isomerase assays were run with a BSA-only control to assess spontaneous isomerization of the substrate. The BSA values were subtracted from the test samples using baseline subtraction. For graphing purposes, the samples were then normalized so that the BSA was set to zero and the SN samples were set to 100%.

Human brain samples and Western blots

Soluble fraction from human brain samples was prepared according to the method of Shankar *et al.* (*2*, *50*). Human brain lysate (35 μg) was run on an Any kD gel (456-9034, Bio-Rad) and transferred to nitrocellulose, blotted, and scanned using Li-Cor Odyssey and analyzed using Image Studio Lite. Antibodies used were Pin1 (SC-46660, Santa Cruz), SNAP25 (ab24737, Abcam), βIII-tubulin (801202, BioLegend), and GAPDH (60004-1-Ig, Proteintech).

Aβ_{42} preparation and concatamerization

Human Aβ_{42} was purchased from Peninsula Laboratories or Bachem America and diluted to 100 μM in 200 mM Hepes (pH 8.0). The solution was gently agitated for 48 hours at RT, aliquoted, and stored at −80°C. The resultant Aβ_{42} was analyzed by Western blot for concatamerization (fig. S2C) (*50*). Human amyloid B (82E1, Immuno-Biological Laboratories) and β-amyloid 17–24 (4G8, Covance) were used to detect oligomers.

XL bead preparation

Pin1 antibody (MAB2294, R&D Systems) or normal mouse immunoglobulin G (IgG) (SC-2025, Santa Cruz) was immobilized on Protein G Sepharose Fast Flow Beads (P3296, Sigma-Aldrich). Beads were equilibrated in PBS for 1 hour with multiple buffer changes. Antibody was added at 4 μg per 20-μl bead slurry in PBS and allowed to bind overnight at 4°C. Beads were washed three times with fresh 0.2 M sodium borate. Freshly made dimethyl pimelimidate dihydrochloride was then used at 5.5 mg/ml in 0.2 M sodium borate for 40 min at RT to cross-link the antibody to the beads. Beads were rinsed and incubated for 2 hours at RT with 0.2 M ethanolamine. Beads were washed three times with PBS and stored up to 4 weeks.

Lysate preparation

SN lysates were made as described above except no Triton X-100 was added after treatment. Samples were instead pelleted at 5000 rpm for 7.5 min at 4°C, at which point pellets were washed with chilled DPBS with calcium and magnesium (21-0303-CV, Corning). Pellets were then snap-frozen and subsequently stored at −80°C. Pellet pairs from several preparations were thawed on ice and combined with

IP buffer: 1× stimulation buffer [10 mM tris (pH 7), 0.5 mM Na_2HPO_4, 0.4 mM KH_2PO_4, 4 mM $NaHCO_3$, 80 mM NaCl, and 0.25% Triton X-100] plus Halt Protease and Phosphatase Inhibitor (1861280, Thermo Fisher Scientific). Samples underwent three freeze/thaw cycles followed by a 30-min incubation on ice with occasional mixing. Samples were then centrifuged (15,000 rpm, 15 min, 4°C). The supernatant was kept, whereas pellets were suspended in additional IP buffer and the spin was repeated. Supernatants from both spins were combined, and concentration was measured with the Pierce BCA Protein Assay Kit (23227, Thermo Fisher Scientific).

Immunoprecipitation and immunoblotting

Freshly made lysates were precleared with normal mouse IgG-XL beads for 2 hours at 4°C. After a quick spin, the precleared lysates were transferred to new tubes and were incubated overnight with Pin1-XL beads. Beads were washed three times with IP buffer and stored in 2× SDS-polyacrylamide gel electrophoresis loading buffer. MS samples were run on an Any kD gel (456-9034, Bio-Rad) and underwent a Pierce Silver Stain for Mass Spectrometry kit (24600, Thermo Fisher Scientific). A visible band around the size of Pin1 (18 kDa) was excised and sent for PTM analysis, or the entire sample was run 10 mm into a protein gel and excised for analysis of Pin1-interacting proteins by the UTSW Proteomics Core. Protein gel pieces were reduced and alkylated with DTT (20 mM) and iodoacetamide (27.5 mM). A solution of trypsin (0.1 μg/μl) in 50 mM triethylammonium bicarbonate (TEAB) was added to completely cover the gel and allowed to sit on ice, and then 50 μl of 50 mM TEAB was added and the gel pieces were digested overnight (Pierce). After solid-phase extraction cleanup with an Oasis HLB μElution plate (Waters), the resulting peptides were reconstituted in 10 μl of 2% (v/v) acetonitrile (ACN) and 0.1% trifluoroacetic acid in water. Five microliters was injected onto an Orbitrap Fusion Lumos mass spectrometer (Thermo Fisher Scientific) coupled to an UltiMate 3000 RSLCnano liquid chromatography systems (Dionex). Samples were injected onto a 75–μm–inside diameter, 50-cm-long EASY-Spray column (Thermo Fisher Scientific) and eluted with a gradient from 1 to 28% buffer B over 60 min. Buffer A contained 2% (v/v) ACN and 0.1% formic acid in water, and buffer B contained 80% (v/v) ACN, 10% (v/v) trifluoroethanol, and 0.1% formic acid in water. The mass spectrometer operated in positive ion mode with a source voltage of 2.4 kV and an ion transfer tube temperature of 275°C. MS scans were acquired at 120,000 resolution in the Orbitrap, and up to 10 MS/MS spectra were obtained in the ion trap for each full spectrum acquired using higher-energy collisional dissociation for ions with charges 2 to 7. Dynamic exclusion was set for 25 s after an ion was selected for fragmentation.

Raw MS data files were converted to a peak list format and analyzed using the central proteomics facilities pipeline (CPFP), version 2.0.3 (*51*, *52*). Peptide identification was performed using the X!Tandem (*53*) and open MS search algorithm (*54*) search engines against the mouse protein database from UniProt, with common contaminants and reversed decoy sequences appended (*55*). Fragment and precursor tolerances of 20 parts per million and 0.6 Da were specified, and three missed cleavages were allowed. Carbamidomethylation of Cys was set as a fixed modification, and oxidation of Met was set as a variable modification. An additional requirement of two unique peptide sequences per protein was used for protein identification. For phosphorylation analysis, phosphorylation of Ser, Thr, and Tyr was also set as variable modifications, and phosphorylation sites were localized using ModeLS PTM Localization 6 and confirmed by manual interpretation.

Western blotting–IP interaction samples were run on an Any kD gel and transferred to nitrocellulose membrane using Trans-Blot Turbo technology. Blots were blocked in 5% BSA in tris-buffered saline. Membranes were scanned using Li-Cor Odyssey. Antibodies to Pin1 (MAB2294) and Ppp3r1 (AF1348) were purchased from R&D Systems, antibody to Ppp3ca (A300-908A-M) was from Bethyl Laboratories, and antibody to Ppp3cb (PA5-15581) was from Thermo Fisher Scientific.

Calcineurin activity assay

Lysates were made the same day as the Calcineurin Cellular Activity Assay Kit, Colorimetric (207007, Millipore) was performed per the company protocol. Plates were read at A_{620} (absorbance at 620 nm) by a Tecan plate reader Spark 10.

Hippocampal AAV1 stereotactic injection

AAV1.CMV.PI.eGFP.WPRE.bGH and AAV1.CMV.HI.eGFP-Cre.WPRE.SV40 were purchased from the University of Pennsylvania vector core and injected bilaterally into the CA1 of 8-week-old Pin-$1^{fl/fl}$ mice in the UTSW Neuro-Models Facility. In total, 24 mice were used with 3 mice per condition per time point. Mice were sacrificed at 3, 6, 9, or 12 DPI. Mice were anesthetized and perfused with 4% PFA. Brains were postfixed in PFA and then transferred through a series of sucrose gradients. Sections (20 μm) were then cut with a vibratome, stained with 4′,6-diamidino-2-phenylindole (DAPI), and mounted. They were then examined for GFP in the hippocampus. For synapse counts in AAV-injected mice, sections were immunostained for synaptophysin (17785-1-AP, Proteintech) and stained with DAPI. The DAPI staining was used to localize to the CA1 region of the hippocampus. Images were then taken in the apical distal region of the CA1 for synapse analysis. Confocal 0.33-μm *Z* stacks of a least six sections were taken, spines were counted, and colocalization of GFP and synaptophysin was analyzed with ImageJ using the NeuronJ and SynaptJ plugins. Laser capture microdissection was used to isolate tissue from the brains of AAV-injected mice. Regions of infected (green cells) from the hippocampus and uninfected (green negative) from the thalamus were used for DNA genotyping analysis.

Statistical analysis

Experiments were replicated at least three times. Data are means ± SEM. Statistical analysis was performed with Prism (GraphPad) software. Statistical differences between means were analyzed by either an unpaired *t* test or Fisher's LSD test following two-way ANOVA. Statistical significance was defined as $P < 0.05$.

SUPPLEMENTARY MATERIALS

www.sciencesignaling.org/cgi/content/full/11/522/eaap8734/DC1

Fig. S1. Pin1 loss causes spine loss.

Fig. S2. Pin1 successfully recombined in mouse hippocampus after AAV-GFP-Cre.

Fig. S3. Pin1 reconstitution restores mature spine counts in the presence of $A\beta_{42}$.

Fig. S4. FK506 restoration of spines requires Pin1.

Fig. S5. Pin1-S111D restores spine counts in wild-type or knockout cells treated with $A\beta_{42}$.

REFERENCES AND NOTES

1. S. Li, S. Hong, N. E. Shepardson, D. M. Walsh, G. M. Shankar, D. Selkoe, Soluble oligomers of amyloid β-protein facilitate hippocampal long-term depression by disrupting neuronal glutamate uptake. *Neuron* **62**, 788–801 (2009).

2. G. M. Shankar, S. Li, T. H. Mehta, A. Garcia-Munoz, N. E. Shepardson, I. Smith, F. M. Brett, M. A. Farrell, M. J. Rowan, C. A. Lemere, C. M. Regan, D. M. Walsh, B. L. Sabatini, D. J. Selkoe, Amyloid-β protein dimers isolated directly from Alzheimer's brains impair synaptic plasticity and memory. *Nat. Med.* **14**, 837–842 (2008).
3. P.-J. Lu, G. Wulf, X. Z. Zhou, P. Davies, K. P. Lu, The prolyl isomerase Pin1 restores the function of Alzheimer-associated phosphorylated tau protein. *Nature* **399**, 784–788 (1999).
4. T. Kimura, K. Tsutsumi, M. Taoka, T. Saito, M. Masuda-Suzukake, K. Ishiguro, F. Plattner, T. Uchida, T. Isobe, M. Hasegawa, S.-i. Hisanaga, Isomerase Pin1 stimulates dephosphorylation of tau protein at cyclin-dependent kinase (Cdk5)-dependent Alzheimer phosphorylation sites. *J. Biol. Chem.* **288**, 7968–7977 (2013).
5. K. P. Lu, X. Z. Zhou, The prolyl isomerase PIN1: A pivotal new twist in phosphorylation signalling and disease. *Nat. Rev. Mol. Cell Biol.* **8**, 904–916 (2007).
6. R. Antonelli, R. De Filippo, S. Middei, S. Stancheva, B. Pastore, M. Ammassari-Teule, A. Barberis, E. Cherubini, P. Zacchi, Pin1 modulates the synaptic content of NMDA receptors via prolyl-isomerization of PSD-95. *J. Neurosci.* **36**, 5437–5447 (2016).
7. Y.-C. Liou, A. Sun, A. Ryo, X. Z. Zhou, Z. X. Yu, H. K. Huang, T. Uchida, R. Bronson, G. Bing, X. Li, T. Hunter, K. P. Lu, Role of the prolyl isomerase Pin1 in protecting against age-dependent neurodegeneration. *Nature* **424**, 556–561 (2003).
8. L. Pastorino, A. Sun, P. J. Lu, X. Z. Zhou, M. Balastik, G. Finn, G. Wulf, J. Lim, S. H. Li, X. Li, W. Xia, L. K. Nicholson, K. P. Lu, The prolyl isomerase Pin1 regulates amyloid precursor protein processing and amyloid-beta production. *Nature* **440**, 528–534 (2006).
9. C. H. Chen, W. Li, R. Sultana, M. H. You, A. Kondo, K. Shahpasand, B. M. Kim, M. L. Luo, M. Nechama, Y. M. Lin, Y. Yao, T. H. Lee, X. Z. Zhou, A. M. Swomley, D. Allan Butterfield, Y. Zhang, K. P. Lu, Pin1 cysteine-113 oxidation inhibits its catalytic activity and cellular function in Alzheimer's disease. *Neurobiol. Dis.* **76**, 13–23 (2015).
10. P. R. Westmark, C. J. Westmark, S. Wang, J. Levenson, K. J. O'Riordan, C. Burger, J. S. Malter, Pin1 and PKMζ sequentially control dendritic protein synthesis. *Sci. Signal.* **3**, ra18 (2010).
11. S. W. Scheff, D. A. Price, Alzheimer's disease-related alterations in synaptic density: Neocortex and hippocampus. *J. Alzheimer's Dis.* **9**, 101–115 (2006).
12. P. R. Westmark, C. J. Westmark, A. Jeevananthan, J. S. Malter, Preparation of synaptoneurosomes from mouse cortex using a discontinuous percoll-sucrose density gradient. *J. Vis. Exp.* 3196 (2011).
13. A. D. Ivanov, G. R. Tukhbatova, S. V. Salozhin, V. A. Markevich, NGF but not BDNF overexpression protects hippocampal LTP from beta-amyloid-induced impairment. *Neuroscience* **289**, 114–122 (2015).
14. G. G. Farías, I. E. Alfaro, W. Cerpa, C. P. Grabowski, J. A. Godoy, C. Bonansco, N. C. Inestrosa, Wnt-5a/JNK signaling promotes the clustering of PSD-95 in hippocampal neurons. *J. Biol. Chem.* **284**, 15857–15866 (2009).
15. W.-H. Sui, S.-H. Huang, J. Wang, Q. Chen, T. Liu, Z-Y. Chen, Myosin Va mediates BDNF-induced postendocytic recycling of full-length TrkB and its translocation into dendritic spines. *J. Cell Sci.* **128**, 1108–1122 (2015).
16. P.-J. Lu, X. Z. Zhou, Y.-C. Liou, J. P. Noel, K. P. Lu, Critical role of WW domain phosphorylation in regulating phosphoserine binding activity and Pin1 function. *J. Biol. Chem.* **277**, 2381–2384 (2002).
17. L. C. R. Tafoya, M. Mameli, T. Miyashita, J. F. Guzowski, C. F. Valenzuela, M. C. Wilson, Expression and function of SNAP-25 as a universal SNARE component in GABAergic neurons. *J. Neurosci.* **26**, 7826–7838 (2006).
18. M. A. Verdecia, M. E. Bowman, K. P. Lu, T. Hunter, J. P. Noel, Structural basis for phosphoserine-proline recognition by group IV WW domains. *Nat. Struct. Biol.* **7**, 639–643 (2000).
19. T. H. Lee, C. H. Chen, F. Suizu, P. Huang, C. Schiene-Fischer, S. Daum, Y. J. Zhang, A. Goate, R. H. Chen, X. Z. Zhou, K. P. Lu, Death-associated protein kinase 1 phosphorylates Pin1 and inhibits its prolyl isomerase activity and cellular function. *Mol. Cell* **42**, 147–159 (2011).
20. V. Rangasamy, R. Mishra, G. Sondarva, S. Das, T. H. Lee, J. C. Bakowska, G. Tzivion, J. S. Malter, B. Rana, K. P. Lu, A. Kanthasamy, A. Rana, Mixed-lineage kinase 3 phosphorylates prolyl-isomerase Pin1 to regulate its nuclear translocation and cellular function. *Proc. Natl. Acad. Sci. U.S.A.* **109**, 8149–8154 (2012).
21. M. Fang, P. Zhang, Y. Zhao, A. Jin, X. Liu, Aβ mediates Sigma receptor degradation via CaN/NFAT pathway. *Am. J. Transl. Res.* **8**, 3471–3481 (2016).
22. H.-Y. Wu, E. Hudry, T. Hashimoto, K. Kuchibhotla, A. Rozkalne, Z. Fan, T. Spires-Jones, H. Xie, M. Arbel-Ornath, C. L. Grosskreutz, B. J. Bacskai, B. T. Hyman, Amyloid β induces the morphological neurodegenerative triad of spine loss, dendritic simplification, and neuritic dystrophies through calcineurin activation. *J. Neurosci.* **30**, 2636–2649 (2010).
23. A. Rozkalne, B. T. Hyman, T. L. Spires-Jones, Calcineurin inhibition with FK506 ameliorates dendritic spine density deficits in plaque-bearing Alzheimer model mice. *Neurobiol. Dis.* **41**, 650–654 (2011).
24. E. C. Miller, L. Zhang, B. W. Dummer, D. R. Cariveau, H. Loh, P. Y. Law, D. Liao, Differential modulation of drug-induced structural and functional plasticity of dendritic spines. *Mol. Pharmacol.* **82**, 333–343 (2012).
25. M. M. Dorostkar, C. Zou, L. Blazquez-Llorca, J. Herms, Analyzing dendritic spine pathology in Alzheimer's disease: Problems and opportunities. *Acta Neuropathol.* **130**, 1–19 (2015).
26. R. Ranganathan, K. P. Lu, T. Hunter, J. P. Noel, Structural and functional analysis of the mitotic rotamase Pin1 suggests substrate recognition is phosphorylation dependent. *Cell* **89**, 875–886 (1997).
27. G. M. Shankar, D. M. Walsh, Alzheimer's disease: Synaptic dysfunction and Aβ. *Mol. Neurodegener.* **4**, 48 (2009).
28. M.-C. Galas, P. Dourlen, S. Bégard, K. Ando, D. Blum, M. Hamdane, L. Buée, The peptidylprolyl *cis/trans*-isomerase Pin1 modulates stress-induced dephosphorylation of Tau in neurons. Implication in a pathological mechanism related to Alzheimer disease. *J. Biol. Chem.* **281**, 19296–19304 (2006).
29. K. Nakamura, I. Kosugi, D. Y. Lee, A. Hafner, D. A. Sinclair, A. Ryo, K. P. Lu, Prolyl isomerase Pin1 regulates neuronal differentiation via β-catenin. *Mol. Cell. Biol.* **32**, 2966–2978 (2012).
30. G. M. Shankar, B. L. Bloodgood, M. Townsend, D. M. Walsh, D. J. Selkoe, B. L. Sabatini, Natural oligomers of the Alzheimer amyloid-β protein induce reversible synapse loss by modulating an NMDA-type glutamate receptor-dependent signaling pathway. *J. Neurosci.* **27**, 2866–2875 (2007).
31. L. J. Sosa, J. S. Malter, J. Hu, F. B. Plonka, M. Oksdath, A. F. N. Guil, S. Quiroga, K. H. Pfenninger, Protein interacting with NIMA (never in mitosis A)-1 regulates axonal growth cone adhesion and spreading through myristoylated alanine-rich C kinase substrate isomerization. *J. Neurochem.* **137**, 744–755 (2016).
32. A. Demuro, E. Mina, R. Kayed, S. C. Milton, I. Parker, C. G. Glabe, Calcium dysregulation and membrane disruption as a ubiquitous neurotoxic mechanism of soluble amyloid oligomers. *J. Biol. Chem.* **280**, 17294–17300 (2005).
33. F. Liu, I. Grundke-Iqbal, K. Iqbal, Y. Oda, K. Tomizawa, C. X. Gong, Truncation and activation of calcineurin A by calpain I in Alzheimer disease brain. *J. Biol. Chem.* **280**, 37755–37762 (2005).
34. G. Taglialatela, C. Rastellini, L. Cicalese, Reduced incidence of dementia in solid organ transplant patients treated with calcineurin inhibitors. *J. Alzheimers Dis.* **47**, 329–333 (2015).
35. H.-Y. Wu, E. Hudry, T. Hashimoto, K. Uemura, Z.-Y. Fan, O. Berezovska, C. L. Grosskreutz, B. J. Bacskai, B. T. Hyman, Distinct dendritic spine and nuclear phases of calcineurin activation after exposure to amyloid-β revealed by a novel fluorescence resonance energy transfer assay. *J. Neurosci.* **32**, 5298–5309 (2012).
36. K. T. Dineley, R. Kayed, V. Neugebauer, Y. Fu, W. Zhang, L. C. Reese, G. Taglialatela, Amyloid-β oligomers impair fear conditioned memory in a calcineurin-dependent fashion in mice. *J. Neurosci. Res.* **88**, 2923–2932 (2010).
37. S. Ikegami, A. Kato, Y. Kudo, T. Kuno, F. Ozawa, K. Inokuchi, A facilitatory effect on the induction of long-term potentiation in vivo by chronic administration of antisense oligodeoxynucleotides against catalytic subunits of calcineurin. *Brain Res. Mol. Brain Res.* **41**, 183–191 (1996).
38. R. M. Mulkey, S. Endo, S. Shenolikar, R. C. Malenka, Involvement of a calcineurin/inhibitor-1 phosphatase cascade in hippocampal long-term depression. *Nature* **369**, 486–488 (1994).
39. G. Malleret, U. Haditsch, D. Genoux, M. W. Jones, T. V. Bliss, A. M. Vanhoose, C. Weitlauf, E. R. Kandel, D. G. Winder, I. M. Mansuy, Inducible and reversible enhancement of learning, memory, and long-term potentiation by genetic inhibition of calcineurin. *Cell* **104**, 675–686 (2001).
40. C. Weitlauf, D. Winder, Calcineurin, synaptic plasticity, and memory. *ScientificWorldJournal* **1**, 530–533 (2001).
41. M. Zhuo, W. Zhang, H. Son, I. Mansuy, R. A. Sobel, J. Seidman, E. R. Kandel, A selective role of calcineurin Aα in synaptic depotentiation in hippocampus. *Proc. Natl. Acad. Sci. U.S.A.* **96**, 4650–4655 (1999).
42. J. Liu, J. D. Farmer Jr., W. S. Lane, J. Friedman, I. Weissman, S. L. Schreiber, Calcineurin is a common target of cyclophilin-cyclosporin A and FKBP-FK506 complexes. *Cell* **66**, 807–815 (1991).
43. J. P. Steiner, M. A. Connolly, H. L. Valentine, G. S. Hamilton, T. M. Dawson, L. Hester, S. H. Snyder, Neurotrophic actions of nonimmunosuppressive analogues of immunosuppressive drugs FK506, rapamycin and cyclosporin A. *Nat. Med.* **3**, 421–428 (1997).
44. D. Tedesco, L. Haragsim, Cyclosporine: A review. *J. Transplant.* **2012**, 230386 (2012).
45. C. R. Overk, E. Rockenstein, J. Florio, Q. Cheng, E. Masliah, Differential calcium alterations in animal models of neurodegenerative disease: Reversal by FK506. *Neuroscience* **310**, 549–560 (2015).
46. F. Eckerdt, J. Yuan, K. Saxena, B. Martin, S. Kappel, C. Lindenau, A. Kramer, S. Naumann, S. Daum, G. Fischer, I. Dikic, M. Kaufmann, K. Strebhardt, Polo-like kinase 1-mediated phosphorylation stabilizes Pin1 by inhibiting its ubiquitination in human cells. *J. Biol. Chem.* **280**, 36575–36583 (2005).
47. M. Jiang, G. Chen, High Ca^{2+}–phosphate transfection efficiency in low-density neuronal cultures. *Nat. Protoc.* **1**, 695–700 (2006).

48. S. Sun, H. Zhang, J. Liu, E. Popugaeva, N. J. Xu, S. Feske, C. L. White III, I. Bezprozvanny, Reduced synaptic STIM2 expression and impaired store-operated calcium entry cause destabilization of mature spines in mutant presenilin mice. *Neuron* **82**, 79–93 (2014).
49. A. Rodriguez, D. B. Ehlenberger, D. L. Dickstein, P. R. Hof, S. L. Wearne, Automated three-dimensional detection and shape classification of dendritic spines from fluorescence microscopy images. *PLOS ONE* **3**, e1997 (2008).
50. G. M. Shankar, A. T. Welzel, J. M. McDonald, D. J. Selkoe, D. M. Walsh, Isolation of low-n amyloid β-protein oligomers from cultured cells, CSF, and brain. *Methods Mol. Biol.* **670**, 33–44 (2011).
51. D. C. Trudgian, H. Mirzaei, Cloud CPFP: A shotgun proteomics data analysis pipeline using cloud and high performance computing. *J. Proteome Res.* **11**, 6282–6290 (2012).
52. D. C. Trudgian, B. Thomas, S. J. McGowan, B. M. Kessler, M. Salek, O. Acuto, CPFP: A central proteomics facilities pipeline. *Bioinformatics* **26**, 1131–1132 (2010).
53. R. Craig, R. C. Beavis, TANDEM: Matching proteins with tandem mass spectra. *Bioinformatics* **20**, 1466–1467 (2004).
54. L. Y. Geer, S. P. Markey, J. A. Kowalak, L. Wagner, M. Xu, D. M. Maynard, X. Yang, W. Shi, S. H. Bryant, Open mass spectrometry search algorithm. *J. Proteome Res.* **3**, 958–964 (2004).
55. J. E. Elias, S. P. Gygi, Target-decoy search strategy for increased confidence in large-scale protein identifications by mass spectrometry. *Nat. Methods* **4**, 207–214 (2007).

Acknowledgments: We thank the UTSW Neuropathology Core of the Alzheimer Disease Center (P30 AG12300) for the brain tissue; the UTSW Proteomics Core (CPRIT RP120613) for the MS analysis; the UTSW Live Cell Imaging Facility, a Shared Resource of the Harold C. Simmons Cancer Center (supported in part by National Cancer Institute Cancer Center Support Grant 1P30 CA142543-01), the UTSW Whole Brain Microscopy Facility (supported by the Texas Institute for Brain Injury and Repair), and the Neuro-Models Facility Core (supported by the Texas Institute for Brain Injury and Repair and the Haggerty Center for Research on Brain Injury and Repair in Stroke) for technical assistance; and members of the UTSW AD research group for their comments and suggestions. We would like to specially thank J. Shelton of UTSW Histo-Pathology Core for his assistance with laser microdissection of cells in the brain. **Funding:** This work was supported by the Senator Betty and Dr. Andy Andujar Endowment and the NIH (P01HL88594 to J.S.M. and R01AG055577 to I.B. and E.T.K.). **Author contributions:** N.R.S., M.A.O., E.T.K., I.B., and J.S.M. designed the project. N.R.S. and M.A.O. performed the experiments and analyzed the data along with J.S.M. J.H. generated and maintained the $Pin^{fl/fl}$ mice. N.R.S., M.A.O., and J.S.M. wrote the manuscript with contributions from E.T.K. and I.B. All authors commented on and approved the final version. **Competing interests:** I.B. is a consultant for Teva Pharmaceutical Industries. The other authors declare that they have no competing interests. **Data and materials availability:** The MS data have been deposited to MassIVE data repository (https://massive.ucsd.edu), accession ID MSV000082066. All other data necessary for interpretation have been shown in the article or in the Supplementary Materials.

Submitted 5 September 2017
Accepted 20 February 2018
Published 20 March 2018
10.1126/scisignal.aap8734

Citation: N. R. Stallings, M. A. O'Neal, J. Hu, E. T. Kavalali, I. Bezprozvanny, J. S. Malter, Pin1 mediates $A\beta_{42}$-induced dendritic spine loss. *Sci. Signal.* **11**, eaap8734 (2018).

Science Signaling

Pin1 mediates Aβ_{42}-induced dendritic spine loss

Nancy R. Stallings, Melissa A. O'Neal, Jie Hu, Ege T. Kavalali, Ilya Bezprozvanny and James S. Malter

Sci. Signal. **11** (522), eaap8734.
DOI: 10.1126/scisignal.aap8734

Pinpointing amyloid's toxicity

An increase in the amount of amyloid-β (Aβ) in neurons alters calcium signaling and causes synaptic dysfunction and dendritic spine loss, which is believed to cause neurodegeneration and cognitive deficits in Alzheimer's disease (AD). The decreased activity of Pin1, a protein that structurally alters the function of serine- and threonine-phosphorylated proteins (including amyloid precursor protein and tau in the postsynaptic space of neurons), is also associated with AD. Using mouse models of AD, Stallings *et al.* found that Pin1 was dephosphorylated and inactivated by the calcium-dependent phosphatase calcineurin, whose activity in postsynaptic neurons was induced by A β. Aβ-induced spine loss was prevented by treating mice with the calcineurin inhibitor FK506 (also known as tacrolimus), an immunosuppressant used to reduce the rejection of organ transplants, suggesting that this drug might be repurposed to treat patients with AD.